

# Electromagnetically induced transparency in inhomogeneously broadened $\Lambda$ -transition with multiple excited levels

O.S. Mishina<sup>1</sup>, M. Scherman<sup>1</sup>, P. Lombardi<sup>1</sup>, J. Ortalo<sup>1</sup>, D. Felinto<sup>2</sup>,

A.S. Sheremet<sup>3</sup>, A. Bramati<sup>1</sup>, D.V. Kupriyanov<sup>3</sup>, J. Laurat<sup>1</sup>, and E. Giacobino<sup>1</sup>

<sup>1</sup>*Laboratoire Kastler Brossel, Université Pierre et Marie Curie, Ecole Normale Supérieure, CNRS, Case 74, 4 place Jussieu, 75252 Paris Cedex 05, France*

<sup>2</sup>*Departamento de Física, Universidade Federal de Pernambuco, 50670-901 Recife, PE, Brazil*

<sup>3</sup>*Department of Theoretical Physics, State Polytechnic University, 195251, St.-Petersburg, Russia*

Electromagnetically induced transparency (EIT) has mainly been modelled for three-level systems. In particular, a considerable interest has been dedicated to the  $\Lambda$ -configuration, with two ground states and one excited state. However, in the alkali-metal atoms, which are commonly used, hyperfine interaction in the excited state introduces several levels which simultaneously participate in the scattering process. When the Doppler broadening is comparable with the hyperfine splitting in the upper state, the three-level  $\Lambda$  model does not reproduce the experimental results. Here we theoretically investigate the EIT in a hot vapor of alkali-metal atoms and demonstrate that it can be strongly reduced due to the presence of multiple excited levels. Given this model, we also show that a well-designed optical pumping enables to significantly recover the transparency.

PACS numbers: 42.50.Gy, 42.50.Ct, 32.80.Qk, 03.67.-a

## I. INTRODUCTION

Electromagnetically induced transparency (EIT), i.e. the fact that a strong field resonant with an atomic transition can make the atomic medium transparent for another field resonant with a transition sharing the same excited state, has been intensively studied for the last two decades [1, 2]. It has given rise to important applications such as Doppler-free spectroscopy, high-precision magnetometry, and lasing without inversion [3]. EIT also led to the demonstration of slow-light [4]. This opened the way to the development of a reversible memory for light based on dynamic EIT, which was first demonstrated for classical pulses in optically dense atomic media [5, 6]. In the framework of quantum information processing and networking, which relies critically on such memories [7–9], these works have been extended to the storage of single-photon pulses [10, 11]. Further developments have resulted in the demonstration of reversible mapping of single-photon entanglement into and out of a quantum memory [12]. In the regime of continuous variables, notable advances have been the storage of squeezed light [13, 14] and the storage in an alkali-metal vapor of a faint coherent pulse retrieved without added excess noise [15, 16].

The performances of the EIT-based memories are limited by several sources of losses. Theoretical models usually rely on a three-level system in a  $\Lambda$  configuration: two atomic ground states are connected to the same excited state via a control field on one transition and a signal field on the other one. In general, these models take into account the losses occurring when the optical depth is not sufficient for a full pulse compression in the medium, which leads to some non-zero transmittance during pulse storage, and also the losses due to atomic ground state decoherence [17, 18]. However, it must be noted that the

experimental demonstrations of such optical and quantum memories were mostly performed in ensembles of alkali-metal atoms. In this case, the level structure is more complex than the simple three-level  $\Lambda$  approximation due to the hyperfine interaction, and the two ground states are often coupled to two, three or even more excited states by the laser fields. In many cases, the excited levels are quite close to each other and the inhomogeneous broadening is comparable with the hyperfine splitting, such as for example in the  $D_2$ -line of cesium atoms. This complex structure may strongly modify the EIT dynamics. Indeed, it has been experimentally demonstrated that the EIT can completely disappear when the inhomogeneous broadening is larger than the hyperfine splitting in the excited state [19]. More generally, in many experimental studies, the transparency is smaller than the value predicted by a three-level theoretical model. The aim of this paper is thus to go beyond the usual three-level  $\Lambda$  approximation and investigate in particular the effect of the inhomogeneous broadening in this case.

Several theoretical studies of EIT have taken into account a double  $\Lambda$ -system with two excited levels in the context of a four-wave mixing process [20–22], which leads to lasing without inversion and squeezed light generation [17]. In these models four levels are considered to be coupled with the fields but each pair of fields is coupled with only one of the  $\Lambda$ -channels. Some investigations have also addressed a different regime where the two fields are allowed to transfer the atom into a superposition of two excited states. They have demonstrated inhibition or enhancement of the off-resonant Raman transition [23–28]. Numerical analysis of the field transmission through an inhomogeneously broadened medium of alkali-metal atoms in Ref. [29] has also shown that several absorption peaks can be observed due to the velocity selective optical pumping via several excited states. A shift of the EIT window from the two-photon resonance

and a partial reduction of the transparency due to the presence of the second excited state were observed and theoretically justified in Refs. [4, 30, 31]. These studies show that several effects may deeply modify the properties of the EIT as compared to the predictions of a simple  $\Lambda$  system.

In this paper, we present a general analysis of EIT addressing both the case of an inhomogeneously broadened medium and that of several  $\Lambda$  transitions due to multiple excited levels. We derive a full analytical expression for the atomic susceptibility that shows evidence for the interference between multiple  $\Lambda$  transitions and unusual velocity dependent light shifts of the resonances. In a situation for which the Doppler broadening of the medium is larger than the separation between different excited states, these effects are responsible for turning the transparency into absorption for some velocity groups of atoms, which significantly reduces the EIT peak in such system. This reduction is commonly observed in EIT experiments on the  $D_2$  line of alkaline atoms for vapors at room temperature [15, 19, 32, 33]. We show that such effect could cause complete disappearance of the EIT peak, if the atoms with reduced transparency were not optically pumped to levels not participating in the EIT process. Once the crucial role of optical pumping in the system is clarified, we devise a new optical pumping scheme to significantly enhance the EIT peak in room temperature atomic vapors. Even though our discussion is focused on the excitation of alkaline atoms, our model can be applied as well to various atom-like physical systems presenting large inhomogeneous broadening and multiple excited levels.

The paper is organized as follows. In Sec. II, the theoretical model is presented. Section III gives the absorption profile of a single atom with multiple excited states. We demonstrate that this profile is strongly dependent on the velocity of the atom. In Sec. IV, we then consider an ensemble of atoms with different velocities and demonstrate that the inhomogeneous broadening leads to a drastic decrease of the transparency. Finally, in Sec. V, we present a possible method to enhance the transparency in such configurations by an effective cooling mechanism based on optical pumping. Section VI gives the concluding remarks. The details of the theoretical derivations are presented in Appendices A and B.

## II. $\Lambda$ -TYPE INTERACTION WITH MULTIPLE EXCITED LEVELS

In this section, we study the influence of the atomic excited state structure on a  $\Lambda$ -type interaction between an atom and two light fields. In order to investigate the transmission of a weak probe light through an atomic medium driven by a strong control field, we first derive here an analytical expression for the atomic susceptibility.

### A. A model case: Cesium $D_2$ -line

A multilevel structure appears in particular in the case of atomic levels possessing a hyperfine structure. Here we will consider alkali-metal atoms, which have a non-zero nuclear spin. Optical D-lines transitions  $n^2S_{1/2} \rightarrow n^2P_{1/2}$  ( $D_1$ -line) and  $n^2S_{1/2} \rightarrow n^2P_{3/2}$  ( $D_2$ -line) are split due to the interaction between electron and nuclear spins. In the ground state  $n^2S_{1/2}$  this interaction leads to a hyperfine splitting of several GHz. The splitting in the excited state is smaller and the excited hyperfine levels are separated by few hundreds MHz. We will consider a  $\Lambda$  type interaction (Fig.1) where the two ground states are sublevels of the same hyperfine state. In view of the large hyperfine splitting in the ground state, we can neglect the interaction of the fields with the other hyperfine state. This is not true in the excited state, where we will have to take into account an interaction of the fields with several levels of the hyperfine manifold.

As a specific example, we will consider a cesium atom  $^{133}\text{Cs}$ , which has been widely used for the experimental investigations of light-matter interfacing [8, 18], for high sensitivity magnetometry [34], as well as for precision frequency measurements in atomic clocks [35]. For the  $D_2$  line, the separation between the closest transitions, which is 150 MHz, is approximately the same as the Doppler linewidth in an ensemble of cesium atoms around room temperature (about 300 K). In practice, due to this Doppler broadening, the transitions are not resolved, and, as we will show, the combined action of this broadening and of the hyperfine structure will strongly influence the EIT interaction.

### B. Basic assumptions and energy levels

The scheme of the light-atom interaction in the  $D_2$ -line of  $^{133}\text{Cs}$  atoms is sketched in Fig. 1. For a rigorous study of the multilevel structure influence on the EIT effect we consider a six-level model, since at least six levels are actually involved in the interaction. State  $|g\rangle \equiv |F=3, m=3\rangle$  is coupled with the excited states  $|e_2\rangle \equiv |F'=2, m=2\rangle$ ,  $|e_3\rangle \equiv |F'=3, m=2\rangle$  and  $|e_4\rangle \equiv |F'=4, m=2\rangle$  by a weak  $\sigma^-$  polarized probe field. A second set of atomic transitions is excited by the strong  $\sigma^+$  polarized control field coupling the ground state  $|s\rangle \equiv |F=3, m=1\rangle$  with the same excited states  $|e_2\rangle, |e_3\rangle, |e_4\rangle$  as the probe field. The detunings of the probe with frequency  $\omega_p$  and control field with frequency  $\omega_c$  from the atomic transitions  $|g\rangle \rightarrow |e_2\rangle$  and  $|s\rangle \rightarrow |e_2\rangle$  will be denoted respectively  $\Delta_p = \omega_p - \omega_{e_2g}$  and  $\Delta_c = \omega_c - \omega_{e_2s}$ . We will assume the control field to be close to resonance with the  $|s\rangle \rightarrow |e_2\rangle$  transition. Let us point out that the dipole moment of the transition  $|g\rangle \rightarrow |e_2\rangle$  is the largest of the three transitions  $|g\rangle \rightarrow |e_i\rangle$  accessible to the probe field.

In addition to the  $\Lambda$ -type interactions, the control field can couple the states  $|g\rangle$  and  $|e\rangle \equiv |F'=4, m=4\rangle$ . As

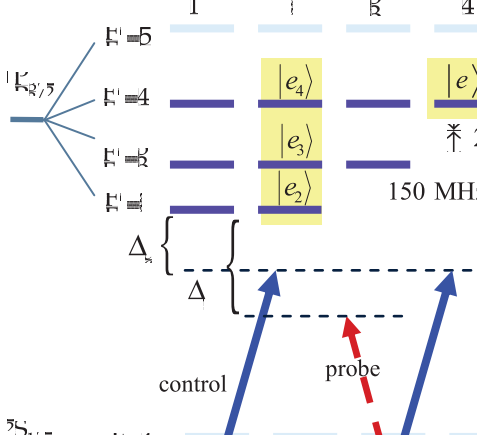


FIG. 1: (color online) Level scheme of  $^{133}\text{Cs}$   $D_2$ -line. In the six-level model, we include the excited levels  $|e_2\rangle$ ,  $|e_3\rangle$ ,  $|e_4\rangle$ ,  $|e\rangle$  and the ground levels  $|s\rangle$  and  $|g\rangle$ . The three-level approximation involves the ground levels  $|s\rangle$ ,  $|g\rangle$  and only  $|e_2\rangle$  as an excited level.

the control field is close to resonance with the  $|s\rangle \rightarrow |e_2\rangle$  transition, this term will be small, but we will see that it can have a non negligible effect. From this section up to Sec. V, we do not consider the decay of the excited levels to the  $F = 4$  cesium ground state, since our aim here is to highlight the role of the interference between different excitation pathways. In Sec. V, the optical pumping to the  $F = 4$  ground state will be taken into account in order to discuss more realistic experimental situations.

Finally, we will compare the six-level model to the simple three-level approximation consisting of the ground states  $|g\rangle$  and  $|s\rangle$ , and only one excited state  $|e_2\rangle$ .

### C. Equations for the six-level model

For the six-level model, the interaction process can be described by the following Hamiltonian  $H$ :

$$H = H_0 + V = H_{\text{field}} + H_{\text{atom}} + V \quad (2.1)$$

with

$$\begin{aligned} V &= V_p + V_c \\ V_p &= - \sum_{F'=2}^4 d_{e_{F'}g} |e_{F'}\rangle \langle g| E_p^{(+)} + h.c. \\ V_c &= - \sum_{F'=2}^4 d_{e_{F'}s} |e_{F'}\rangle \langle s| E_c^{(+)} - d_{eg} |e\rangle \langle g| E_c^{(+)} + h.c. \end{aligned} \quad (2.2)$$

The Hamiltonian  $H_0$  is given by the sum of the free Hamiltonian operators of the electromagnetic field  $H_{\text{field}}$  and of the atom  $H_{\text{atom}}$ . The interaction Hamiltonian  $V$  is written in the rotating wave approximation and consists

in the dipole interactions between the atom and the control and probe fields. In the interaction representation, the positive frequency components of the electromagnetic field for the control and probe modes are  $E_c^{(+)} = \varepsilon_c e^{-i\omega_c t}$  and  $E_p^{(+)} = \varepsilon_p e^{-i\omega_p t}$  respectively;  $d_{ij}$  is the matrix elements of the electric dipole moment of the atom between levels  $i$  and  $j$ .

The response of the atom to the weak probe field is described by the polarizability  $\alpha(\Delta_c, \Delta_p)$  defined as

$$\alpha(\Delta_c, \Delta_p) \varepsilon_p = \sum_{F'=2}^4 d_{g e_{F'}} \sigma_{e_{F'}g}. \quad (2.3)$$

The right-hand side is written as a function of the steady state solutions for the slowly varying amplitudes of the optical coherence between the ground and the excited states addressed by the probe field, which are given by :

$$\sigma_{e_{F'}g} = \rho_{e_{F'}g} e^{i\omega_p t}, \quad (2.4)$$

where  $\rho_{e_{F'}g}$  (with  $F' = 2, 3, 4$ ) are the corresponding atomic density matrix elements. In the case of a dilute atomic system, when the number of atoms in a volume of a cubic wavelength is small, the complex susceptibility is proportional to the single atom polarizability

$$\chi(\Delta_c, \Delta_p) = n_0 \alpha(\Delta_c, \Delta_p) \quad (2.5)$$

with  $n_0$  the atomic density.

The matrix elements of the atomic density matrix  $\rho_{ig}$  will be found in the semiclassical approach as a steady state solution of the evolution equation up to the first order with respect to the probe field  $\rho_{e_{F'}g} = \rho_{e_{F'}g}^{(0)} + \rho_{e_{F'}g}^{(1)}$ . In the operator form one needs subsequently to solve the following master equations

$$\begin{aligned} \frac{d\rho^{(0)}}{dt} &= \frac{i}{\hbar} [\rho^{(0)}, H_{\text{atom}} + V_c] + \Gamma(\rho^{(0)}) \\ \frac{d\rho^{(1)}}{dt} &= \frac{i}{\hbar} [\rho^{(0)}, V_p] + \frac{i}{\hbar} [\rho^{(1)}, H_{\text{atom}} + V_c] + \Gamma(\rho^{(1)}). \end{aligned} \quad (2.6)$$

$\Gamma$  is a relaxation operator describing the radiative decay of the excited states as well as decoherence processes in the ground states, as detailed in Appendix A.

Here, we assume that the decoherence in the ground states is much slower than the decay of the excited states. For instance, in a cesium vapor cell with a few centimeters in diameter at room temperature, the free flight time  $\tau_d$  of the atom through the beam is on the order of hundreds of microseconds, which is orders of magnitude larger than the excited state decay time (tens of nanoseconds). In the following, we will assume  $\tau_d = 300 \mu\text{s}$ . In this case the strong control field optically pumps the atoms in the state with  $m_F = 3$  for the hyperfine sublevel  $F = 3$ , i.e. in state  $|g\rangle$ , and state  $|F = 3, m_F = 1\rangle$ , i.e. state  $|s\rangle$  is empty. The zero order density matrix, presented in details in Appendix A, has thus only three non-negligible elements  $\rho_{gg}^{(0)}$ ,  $\rho_{ge}^{(0)}$  and  $\rho_{ee}^{(0)}$ . However, since we

have assumed that the control field is far detuned from the  $|g\rangle \rightarrow |e\rangle$  atomic transition, we can take  $\rho_{gg}^{(0)} \approx 1$  and  $\rho_{ge}^{(0)} \approx \rho_{ee}^{(0)} \approx 0$ . This approximation is justified for Cesium vapors at room temperature since the Doppler broadening half width at half maximum is on the order of 150 MHz and the transition  $|g\rangle \rightarrow |e\rangle$  is separated by 350 MHz from the resonant transition  $|s\rangle \rightarrow |e_2\rangle$ , as shown in Fig. 1. On the other hand, in this part of the calculation, as mentioned above, we will not take into account that some atoms decay from the excited states to level  $|F=4\rangle$  in the ground state, and we will assume that the number of atoms involved in our scheme is kept constant. Optical pumping towards the  $|F=4\rangle$  level and repumping towards  $|F=3\rangle$  will be treated explicitly in section V.

Finally, let us note that in our model the atomic coherence lifetime is only set by the diffusion of the atoms out of the light beam, which corresponds for instance to the case of a cell without paraffine coating or buffer gas. Several studies of the EIT in the presence of atomic diffusion including multiple collisions have been given in [36–38], but in a three-level configuration. In order to focus on the multilevel effect, we do not take such diffusion into account here.

#### D. Solution for the three-level approximation

Before solving the six-level model, let us first recall the solution for a three-level system including the ground states  $|g\rangle$  and  $|s\rangle$  and only one excited state  $|e_2\rangle$ . It is obtained from the previous equations by setting to zero the dipole elements with  $F'_1, F'_2 \neq 2$ ,  $d_{se_{F'_1}}$  and  $d_{ge_{F'_2}}$ . The coherence then takes the following form [17, 39]:

$$\sigma_{e_2g}^{(1)} = -\frac{\rho_{gg}^{(0)}}{2\Delta_{e_2g}} \left( 1 + \frac{|\Omega_{e_2s}^c|^2}{4\Delta_{sg}\Delta_{e_2g}} \right) \Omega_{e_2g}^p. \quad (2.7)$$

The atomic coherence depends on the one- and two-photon detunings through

$$\begin{aligned} \Delta_{e_2g} &= i\gamma_{e_2g} + \Delta_p \\ \Delta_{sg} &= i\gamma_{sg} + \Delta_p - \Delta_c - \frac{|\Omega_{se_2}^c|^2}{4\Delta_{e_2g}}. \end{aligned} \quad (2.8)$$

Here  $\Omega_{e_{F'}s}^c = 2d_{e_{F'}s}\varepsilon_c/\hbar$  and  $\Omega_{e_{F'}g}^p = 2d_{e_{F'}g}\varepsilon_p/\hbar$  (with  $e_{F'} = e_2$ ) are the Rabi frequencies of the control and the probe fields, respectively. The optical coherence relaxation rate is  $\gamma_{e_{F'}g} \approx \gamma/2$  where  $\gamma = 2\pi \times 5.2$  MHz is the decay rate of the atomic excited state in the  $D_2$ -line of  $^{133}\text{Cs}$  atom and  $\gamma_{sg}$  is the decay rate of the ground state coherence  $\sigma_{sg}$ . This expression gives the well-known dressed atom levels, with a splitting (Autler-Townes splitting [43]) of the excited state in two levels separated by  $\Omega_{e_{F'}s}^c$  as well as the EIT at  $\Delta_p = 0$  when  $\Delta_c = 0$ . We now turn to the multiple level case.

#### E. Solution for the six-level model

In the model studied here, which includes four excited states, the solution for the atomic coherences takes the following form

$$\begin{aligned} \sigma_{e_{F'}g}^{(1)} &= -\frac{\rho_{gg}^{(0)}}{2\Delta_{e_{F'}g}} \left( 1 + \frac{|\Omega_{e_{F'}s}^c|^2}{4\Delta_{sg}\Delta_{e_{F'}g}} \right) \Omega_{e_{F'}g}^p \\ &\quad - \frac{\rho_{gg}^{(0)}\Omega_{e_{F'}s}^c}{2\Delta_{sg}\Delta_{e_{F'}g}} \sum_{F'_1 \neq F'} \frac{\Omega_{se_{F'_1}}^c}{4\Delta_{e_{F'_1}g}} \Omega_{e_{F'_1}g}^p \\ &\quad - \rho_{gg}^{(0)} N_{e_{F'}g} \frac{\varepsilon_p}{\hbar} \end{aligned} \quad (2.9)$$

where  $F'$  and  $F'_1$  run through the excited states  $F', F'_1 = 2, 3, 4$ .

The first line coincides with the solution for the three-level system given in Eq. (2.8). The second line comes from the presence of several levels in the excited state of the atom, which introduces additional contributions that can interfere constructively or destructively with the direct contribution given in the first line. In the third line, the quantity  $N_{e_{F'}g}$  represents the contribution of the excited state  $|e\rangle$  which is small since the control field is far from resonance with the  $|g\rangle \rightarrow |e\rangle$  transition, as stated above. An explicit expression for  $N_{e_{F'}g}$  is given in the Appendix A.

An important change relative to the three-level model is also the modification of the detuning term  $\Delta_{sg}$  in the denominator of Eq. (2.9), which will generate additional shifts in the position of the dressed atom levels. The denominators appearing in Eq. (2.9) can now be written as:

$$\begin{aligned} \Delta_{sg} &= i\gamma_{sg} + \Delta_p - \Delta_c - \sum_{F'} \frac{|\Omega_{se_{F'}}^c|^2}{4\Delta_{e_{F'}g}} - \frac{|\Omega_{eg}^c|^2}{4\Delta_{se}} - \Delta_N \\ \Delta_{e_{F'}e} &= i\gamma_{e_{F'}e} + \Delta_p - \Delta_c - \omega_{e_{F'}e} + \omega_{sg} - \frac{|\Omega_{ge}^c|^2}{4\Delta_{e_{F'}g}} \\ \Delta_{se} &= i\gamma_{se} + \Delta_p - 2\Delta_c + \omega_{ee_2} + \omega_{sg} - \sum_{F'} \frac{|\Omega_{se_{F'}}^c|^2}{4\Delta_{e_{F'}e}}. \end{aligned} \quad (2.10)$$

Here  $\omega_{ij} = (E_i - E_j)/\hbar$  is the atomic transition frequency between levels  $i$  and  $j$ , and  $E_i$  is the energy of the unperturbed atomic state  $|i\rangle$ ; the optical coherence relaxation rates are  $\gamma_{eg} = \gamma_{es} \approx \gamma/2$  and the excited hyperfine coherence relaxation rate is  $\gamma_{e_{F'}e} = \gamma$ . The expression of  $\Delta_N$  is given in appendix A and similarly to the terms proportional to  $N_{e_{F'}g}$  in Eq. (2.9) it will not play a significant role in our analysis.

Substituting expression (2.9) into equation (2.3) and using equation (2.5) we obtain an analytical expression for the atomic susceptibility:



$$\begin{aligned}
\chi(\Delta_c, \Delta_p) = & -\frac{\rho_{gg}^{(0)} n_0}{\hbar} \sum_{F'} \frac{|d_{e_{F'}g}|^2}{\Delta_{e_{F'}g}} \\
& - \frac{\rho_{gg}^{(0)} n_0}{\hbar \Delta_{sg}} \left( \sum_{F'} \frac{d_{ge_{F'}} \Omega_{e_{F'}s}^c}{2\Delta_{e_{F'}g}} \right)^2 \\
& - \frac{\rho_{gg}^{(0)} n_0}{\hbar} \sum_{F'} d_{ge_{F'}} N_{e_{F'}g}. \quad (2.11)
\end{aligned}$$

The expression in the first line corresponds to the sum of the susceptibilities of independent two-level systems without a control field. The terms in the second line represent the effect of multiple  $\Lambda$  systems. The squared sum in parenthesis shows that the contribution of the various  $\Lambda$  transitions can interfere positively or destructively. It depends on the signs of the products of terms such as  $d_{ge_{F'}} \times d_{e_{F'}s} / \Delta_{e_{F'}g}$  and  $d_{ge_{F''}} \times d_{e_{F''}s} / \Delta_{e_{F''}g}$ , i.e., the dipole moment between states  $|g\rangle$  and  $|e_{F'}\rangle$  coupled by the probe field and multiplied by the dipole moment between states  $|s\rangle$  and  $|e_{F'}\rangle$  coupled by the control field, divided by  $i\gamma$  plus the detuning of the probe field.

To give an example we consider the case of two coupled  $\Lambda$  transitions corresponding to two hyperfine upper states, when both control and probe fields are tuned between the hyperfine levels. In the situation discussed in this paper the control and the probe fields have opposite polarizations. In this case the dipole moments of the neighboring transitions addressed by the probe field have opposite signs. At the same time, the dipole moments of the transitions addressed by the control field have the same signs and the detunings have opposite signs. This leads to a constructive interference and to an enhancement of the induced Raman scattering as shown in reference [26].

Let us underline that expression (2.11) can be easily generalized to various physical multilevel systems. Similar configurations to the hyperfine interaction might appear in rare-earth doped crystals [40], in quantum dots [41] or for NV-centers in diamonds [42].

### III. SUSCEPTIBILITY FOR ATOMS WITH NON-ZERO VELOCITY

The model has been solved in the previous section for an atom with zero velocity. However, many EIT experiments are performed in Doppler broadened media. In order to investigate such configurations, we first look here at the absorption properties of atoms with different velocities.

#### A. Doppler shift

We consider an atom with velocity  $\mathbf{v}$  interacting with the co-propagating control and probe fields. The Doppler

shifts are approximately the same for the control and probe fields, i.e.  $\Delta_D = -\mathbf{k}_c \cdot \mathbf{v} \approx -\mathbf{k}_p \cdot \mathbf{v}$ , where  $\mathbf{k}_c$  and  $\mathbf{k}_p$  are respectively the wave vectors of the control and probe fields. The two-photon detuning between the control and probe field, which is a critical parameter, can be thus considered here as independent of the atomic velocity.

In the following analysis we set the control field detuning from level  $e_2$  equal to zero,  $\Delta_c = 0$ . In this case, the two-photon resonance will appear when the detuning of the probe field  $\Delta_p$  is also close to zero independently of the atomic velocity, corresponding to the two-photon resonance. The atomic absorption profile for different velocity classes is given by the imaginary part of the susceptibility calculated for the corresponding Doppler shifts of the two fields  $\text{Im}[\chi(\Delta_p + \Delta_D, \Delta_c + \Delta_D)]$ , obtained from equation (2.11).

#### B. Case of the $\Lambda$ approximation

Let us first focus on the result for the three-level scheme presented in the first column of Fig. 2. The positions of the two absorption peaks (Autler-Townes doublet [43]) are given by the poles of the atomic susceptibility, which can be obtained by  $\text{Re}[\Delta_{sg}] = 0$ . We will be interested in one of the two poles which appears for small probe field detunings  $|\Delta_p| \ll |\Delta_D|$  and is thus located in the EIT window of atoms with zero Doppler shift. To estimate the position of this pole, we assume  $|\Delta_D| \gg \gamma$ ,  $|\Omega_{e_2s}|$  and we rewrite the expression  $\Delta_{sg}$  from Eq. (2.10) as:

$$\begin{aligned}
\Delta_{sg} = & i\gamma_{sg} + (\Delta_p + \Delta_D) - (\Delta_c + \Delta_D) \\
& - \frac{|\Omega_{se_2}^c|^2}{4(i\gamma_{e_2g} + (\Delta_p + \Delta_D))} \\
\approx & i\gamma_{sg} + \Delta_p - \frac{|\Omega_{se_2}^c|^2}{4(i\gamma_{e_2g} + \Delta_D)} \\
\approx & i \left( \gamma_{sg} + \frac{\gamma}{2} \frac{|\Omega_{se_2}^c|^2}{4\Delta_D^2} \right) + \Delta_p - \frac{|\Omega_{se_2}^c|^2}{4\Delta_D}. \quad (3.1)
\end{aligned}$$

We find that the Autler-Townes absorption resonance (ATR) appears when the probe field detuning is  $\Delta_p \approx \Delta_{ATR}^{3-level}$  with

$$\Delta_p \approx \Delta_{ATR}^{3-level} = \frac{|\Omega_{se_2}^c|^2}{4\Delta_D}. \quad (3.2)$$

This position of the induced absorption resonance for the probe field is thus determined by the dynamic Stark shift of the atomic levels due to the off-resonant interaction with the strong control field. The result of the exact calculation for the absorption spectrum of three level atoms is shown in Fig. 2, first column. The vertical lines indicate the positions of the resonances approximated by the analytical equations (3.2). The shift is positive (blue shift) for atoms traveling in a direction opposite to the lasers ( $\Delta_D > 0$ ), while it is negative (red shift) for atoms

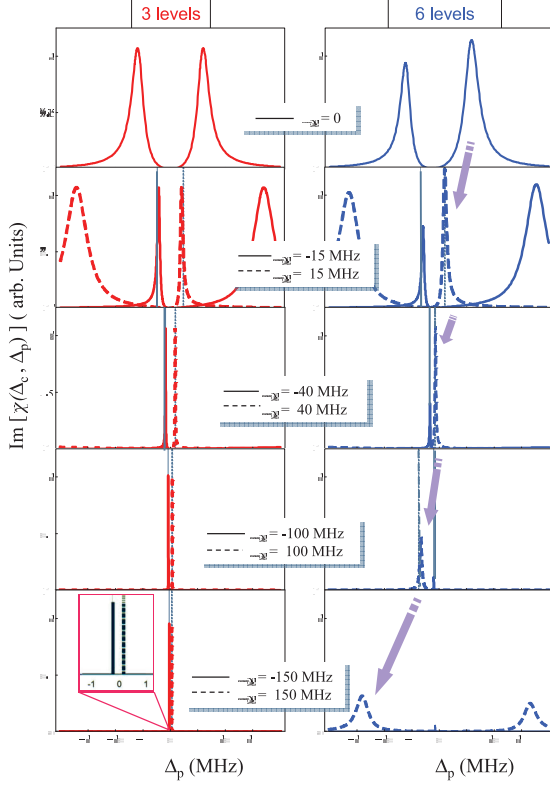


FIG. 2: (color online) Probe absorption coefficient for atoms with different velocities as a function of the probe detuning. Calculations for the three-level and the six-level model are presented respectively in the first and second column. Dashed curves correspond to the velocity classes with positive Doppler shifts ( $\Delta_D > 0$ ) and solid curves correspond to the negative Doppler shifts ( $\Delta_D < 0$ ) with the values indicated in each graph. Vertical lines indicate the positions of the resonances approximated by the analytical equations (3.2) and (3.3), which are in good agreement with the precise numerical calculations. In the three-level system absorption peaks never cross the zero detuning thus the atomic medium is transparent at  $\Delta_p = 0$ . In contrast, the full calculation for the six-level system shows that the induced absorption of atoms from some velocity classes occurs right at the position where other atoms are transparent. In the present calculations the control field detuning is  $\Delta_c = 0$ , the Rabi frequency is  $\Omega_{e_2 s}^c = 2.3\gamma = 2\pi \times 12$  MHz and the ground state decoherence rate is  $\gamma_{sg} = 0.0001\gamma$ .

traveling in the same direction as the lasers ( $\Delta_D < 0$ ).  $\Delta_{ATR}^{3-level}$  can be very small but it must be stressed that it never reaches zero, i.e. the absorption resonance never takes place at zero detuning. Whatever their velocity, the atoms are transparent for the probe field at  $\Delta_p = 0$ .

### C. Case of the full model

As shown in the second column of Fig. 2, the situation is significantly different for the six-level model. The positions of the induced Raman absorption resonances for the probe field are strongly modified. They can be estimated similarly to the three-level case as a real part of the pole of the atomic susceptibility closest to the control laser frequency. By setting to zero the real part of the detuning  $\Delta_{sg}$  from equation (2.10), we find that the absorption resonance appears when the probe field detuning is  $\Delta_p \approx \Delta_{ATR}^{6-level}$  with

$$\Delta_{ATR}^{6-level} = \Delta_{ATR}^{3-level} + \frac{|\Omega_{e_3 s}^c|^2}{4(\Delta_D - \omega_{e_3 e_2})} + \frac{|\Omega_{e_4 s}^c|^2}{4(\Delta_D - \omega_{e_4 e_2})} - \frac{|\Omega_{eg}^c|^2}{4(\Delta_D - \omega_{e e_2} - \omega_{sg})}. \quad (3.3)$$

To derive this expression we assumed that none of the transitions are saturated by the off-resonant control field:

$$\begin{aligned} \Delta_D &\gg \gamma, \Omega_{e_2 s}^c \\ \Delta_D - \omega_{e_3 e_2} &\gg \gamma, \Omega_{e_3 s}^c \\ \Delta_D - \omega_{e_4 e_2} &\gg \gamma, \Omega_{e_4 s}^c. \end{aligned} \quad (3.4)$$

As explicitly written, the first term in the expression (3.3) coincides with the three level approximation (3.2). The second and the third terms show the dynamic Stark shifts due to the presence of the extra excited states  $|e_3\rangle$  and  $|e_4\rangle$ . The last term represents the shift of the state  $|g\rangle$  due to the off-resonant action of the control field on the  $|g\rangle \leftrightarrow |e\rangle$  transition. In the second column of Fig. 2 we compare this estimation, represented by the grey vertical lines, with the exact absorption spectrum calculated numerically for Doppler shifts equal to 20 MHz, 50 MHz and 100 MHz. As can be seen, they coincide very well, which confirms the validity of the approximation made in equation (3.3).

It can be clearly seen in Fig. 2 (second column) that the positions of the induced absorption resonances in the six-level system do not converge to the same point for positive and negative Doppler shifts as they do in the three-level model. For atoms traveling in the same direction as the lasers ( $\Delta_D < 0$ , full lines), the shift of the Autler-Townes absorption resonance always keeps the same negative sign, since  $\omega_{e_3 e_2}$  and  $\omega_{e_4 e_2}$  are positive. On the contrary, for atoms traveling opposite to the light beams ( $\Delta_D > 0$ , dashed lines), the position of the atomic dressed state moves continuously from positive to negative detunings when the Doppler shift increases. For  $\Delta_D = 150$  MHz (right column, bottom curve), the lasers are resonant with level  $e_3$  giving rise to a splitting in two symmetrical dressed levels. Because of this dependence of the absorption resonance positions with respect to velocity, the response of an atomic vapor containing atoms with all these velocity classes is strongly modified.

In Fig. 3, we have plotted the heights of the induced absorption resonances as a function of their positions.

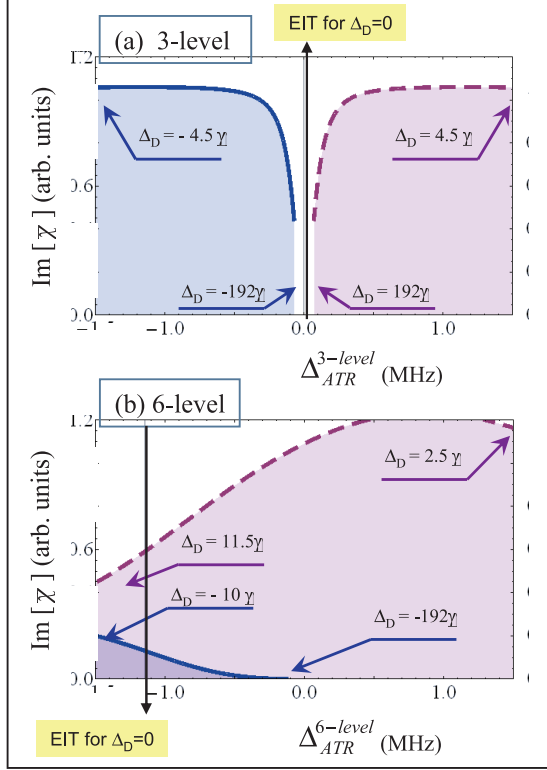


FIG. 3: (color online) Maximum absorption coefficient versus position  $\Delta_{ATR}$  for different velocity classes with Doppler shift  $\Delta_D$ . (a) For the three-level model, the Doppler shift is varied from  $-192\gamma$  ( $-1000$  MHz) to  $-4.5\gamma$  ( $-23$  MHz) (blue, solid line) and from  $4.5\gamma$  to  $192\gamma$  (red, dashed line).  $\Delta_{ATR}^{3-level}$  is an exact solution of  $\text{Re}[\Delta_{sg}] = 0$  for the three-level system. (b) For the six-level model, the Doppler shift is varied from  $-192\gamma$  to  $-10\gamma$  ( $-52$  MHz) (blue, solid line) and from  $2.5\gamma$  ( $13$  MHz) to  $11.5\gamma$  ( $60$  MHz) (red, dashed line).  $\Delta_{ATR}^{6-level}$  is given by Eq. (3.3). The control field is on resonance with level  $|e_2\rangle$ ,  $\Delta_c = 0$ , and the Rabi frequency is  $\Omega_{e_1s} = 2\pi \times 12$  MHz. Vertical lines show the positions of the transparency window for the atoms with zero Doppler shift, which is at  $\Delta_p = 0$  for the 3-level system and which is at  $\Delta_p = -1.15$  MHz for the six-level system according to Eq. (4.3).

The corresponding Doppler shifts are indicated on the curves. Let us first examine the three-level model (Fig. 3(a)). Scanning the Doppler shift from  $-23$  MHz to  $-1000$  MHz, we can see that the position of the absorption resonance approaches zero for large Doppler shift. Simultaneously the maximum absorption decreases due to the dephasing in the ground state. This dephasing comes from the ground state decoherence rate  $\gamma_{sg}$  due to the finite size of the light beam. We set the decoherence to be equal to the inverse atomic time of flight through the light beam  $\gamma_{sg} = 0.0001\gamma$ . For positive Doppler shift the result is completely symmetric relative to the zero point. There is no velocity class producing an induced absorption for  $\Delta_p = 0$  and thus the transparency window re-

mains open even if atoms with all possible Doppler shifts interact with the fields at the same time.

The six-level model is presented in Fig. 3(b). For negative Doppler shifts (blue, solid line), due to the interaction of several  $\Lambda$ -channels, the cross section of the induced Raman scattering is reduced in the wing of the  $D_2$  line. This can be seen from Fig. 2 where the induced absorption resonance almost disappears for  $\Delta_D \leq -100$  MHz. This effect was described in reference [24, 26] for the  $D_1$ -transition in alkali-metal atoms. On the other hand, when the Doppler shift is positive (red, dashed line), the situation changes completely. As could already be seen in Fig. 2, absorption from atoms with non zero Doppler shifts appears for the same probe field detuning as EIT for atoms with zero Doppler shift. The position of the EIT for zero velocity is indicated in Fig. 3(b) by the vertical grey line. We see that the EIT can be strongly reduced by the combined effect of different velocity classes.

To summarize our results, this section shows that it is a unique property of the three-level system that independently of the atomic velocity the EIT appears at the same probe field detuning. This allows for the observation of the EIT even in the presence of a large Doppler broadening [2]. As demonstrated here, this property is not preserved in a system with more than one excited state. There is no longer a probe field detuning for which atoms with different velocities are transparent. This will strongly affect the EIT observation in the six-level system in the presence of a Doppler broadening which is comparable to the separation between the excited states. This situation is described in the following section.

#### IV. EFFECT OF DOPPLER BROADENING ON EIT FOR A SYSTEM WITH MULTIPLE EXCITED LEVELS

At room temperature the Doppler broadening for alkali-metal atoms is comparable with the hyperfine separation between the excited states of the  $D$ -transition, as shown in Table I [44]. This section studies the influence of a finite temperature on the probe transmission in a multiple level configuration.

##### A. Susceptibility of the medium

To find the susceptibility of the sample at a given temperature we average the susceptibility of the atoms  $\chi(\Delta_c + \Delta_D, \Delta_p + \Delta_D)$  over the velocity distribution  $f(\Delta_D)$  for atoms in the ground state  $|g\rangle$ :

$$\bar{\chi}(\Delta_c, \Delta_p) = \int \chi(\Delta_c + \Delta_D, \Delta_p + \Delta_D) f(\Delta_D) d\Delta_D. \quad (4.1)$$

The probe transmittance  $t = |\varepsilon_p(L)|^2 / |\varepsilon_p(0)|^2$  through the medium of length  $L$  is given by the Beer's law:

$$t = \exp(-4\pi k_p L \text{Im}[\bar{\chi}(\Delta_c, \Delta_p)]). \quad (4.2)$$

TABLE I: Doppler broadening and hyperfine splittings for cesium and rubidium atoms at  $T = 300\text{K}$ . The Doppler width is given by  $\Gamma_D = \sqrt{k_B T / m \lambda^2}$  where  $k_B$  is a Boltzmann constant,  $m$  is an atomic mass and  $\lambda$  is a light wavelength.

Atom		$^{133}\text{Cs}$	$^{87}\text{Rb}$	$^{85}\text{Rb}$
Doppler width, MHz		160	198	200
Hyperfine splitting, MHz	$D_1$ -line	1168	817	362
	$D_2$ -line	151	72	29
		201	157	63
		251	267	120

The velocity distribution is assumed to be Gaussian with  $f(\Delta_D) = (2\pi\Gamma_D^2)^{-1/2} \exp(-\Delta_D^2/2\Gamma_D^2)$  where the Doppler width  $\Gamma_D$  depends on the temperature  $T$  of the sample. In Fig. 4 we present the probe transmittance  $t$  as a function of the probe field detuning  $\Delta_p$  for a cesium vapor with different temperatures. For comparison, the figure gives the results for the three-level and the six-level models.

### B. Case of small Doppler broadening

Let us consider first the case of a sample with small Doppler broadening. When the temperature of the medium is  $T = 1\text{ K}$  and the Doppler broadening is  $\Gamma_D = 10\text{ MHz}$ , which is much smaller than the splitting between the closest hyperfine excited states, a clear EIT resonance is predicted by both models. It is indeed well-known that the transparency is present in cold cesium atoms despite the complicated multi-level structure [12]. However, there are some noticeable differences in the predictions of the two models (see Fig. 4).

First, the EIT resonance is shifted from the bare two photon resonance  $\Delta_p = 0$ . This light shift is caused by the presence of the excited states  $|e_3\rangle$ ,  $|e_4\rangle$  and  $|e\rangle$ , as previously explained in references [4, 26] in the case of the  $D_1$ -transition in alkali-metal atoms. In the presence of additional excited states, there are additional dynamic Stark shifts of the dressed states due to the off-resonant interaction with the control field. The EIT resonance is located at the minimum of  $\text{Im}[\sigma_{e_2 g}^{(1)}]$  given by Eq. 2.9. If the separations between the hyperfine transitions are larger than the Rabi frequencies of the control field  $\omega_{e_3 e_2} \gg \Omega_{e_3 s}^c$  and  $\omega_{e_4 e_2} \gg \Omega_{e_4 s}^c$  the EIT position can be approximated

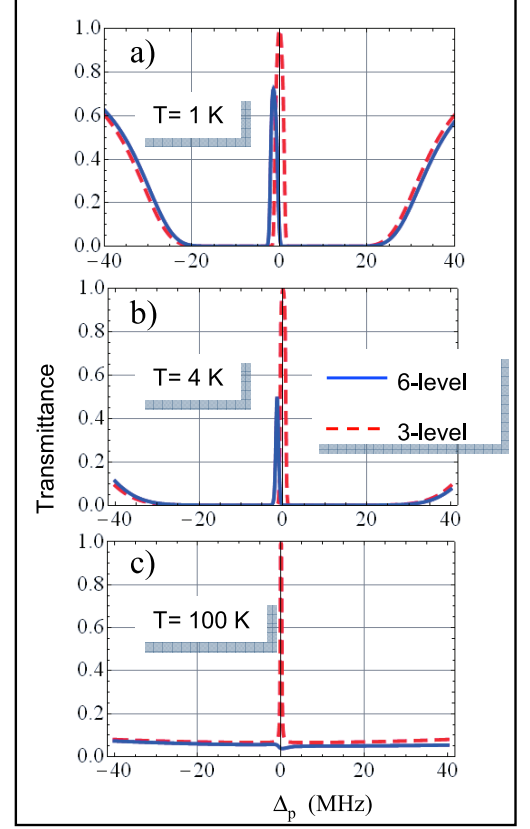


FIG. 4: (color online) Probe field transmittance  $t$  for a Doppler broadened  $D_2$ -line for  $^{133}\text{Cs}$  vapor with equal number of atoms and different temperatures: (a)  $T=1\text{ K}$ ,  $\Gamma_D=10\text{ MHz}$ , (b)  $T=4\text{ K}$ ,  $\Gamma_D=20\text{ MHz}$  and (c)  $T=100\text{ K}$ ,  $\Gamma_D=100\text{ MHz}$ . The control field detuning is  $\Delta_c = 0$  and the Rabi frequency  $\Omega_{e_1 s}^c = 2.3\gamma = 2\pi \times 12\text{ MHz}$ . Calculations are done with the three-level model (dashed, red curves) and the six-level model (solid, blue curves). The atomic density is the same for curves a, b and c and is equal to  $n_0 = 1.1 \times 10^{10}\text{ cm}^{-3}$  with all atoms in state  $|g\rangle$ .

by the following expression:

$$\Delta_{EIT}^{6\text{-level}} = -\frac{|\Omega_{e_3 s}^c|^2}{4\omega_{e_3 e_2}} - \frac{|\Omega_{e_4 s}^c|^2}{4\omega_{e_4 e_2}} + \frac{|\Omega_{eg}^c|^2}{4(\omega_{e e_2} + \omega_{sg})}. \quad (4.3)$$

The first two terms in expression (4.3) represent the shifts of the EIT point due to off-resonance excitations of the states  $|e_3\rangle$  and  $|e_4\rangle$ . The last term corresponds to the shift of the state  $|g\rangle$  due to the action of the off-resonant control field on the  $|g\rangle \leftrightarrow |e\rangle$  transition.

Second, the peak transmittance is reduced in a multi-level configuration. This effect can be explained by the dephasing of the ground state coherence  $\sigma_{sg}$  introduced by the off-resonance excitation of the levels  $F' = 3$  and  $F' = 4$  by the control field. Both effects were observed in Ref. [4] and studied in details in Refs. [26, 30].



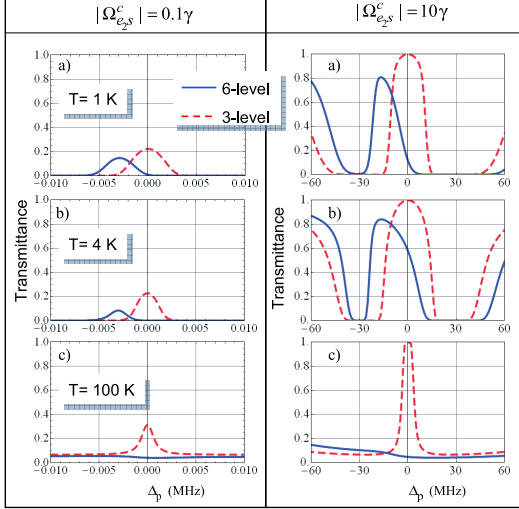


FIG. 5: (color online) Probe field transmittance  $t$  for a Doppler broadened  $D_2$ -line for  $^{133}\text{Cs}$  vapor for different control Rabi frequencies. The parameters and notations are similar than in figure 4. The Rabi frequency is here (left column)  $\Omega_{e1s}^c = 0.1\gamma = 2\pi \times 0.52$  MHz and (right column)  $\Omega_{e1s}^c = 10\gamma = 2\pi \times 52$  MHz. In both cases, large inhomogeneous broadening leads to the total disappearance of the transparency peak. Let us note that the reduced transmittance in the three-level model for small Rabi frequency is due to a reduced ratio between this frequency and the decoherence rate taken equal to  $\gamma_{sg} = 0.0001\gamma$  in all the simulations.

### C. Case of broadening of the order of the hyperfine splitting

If we increase the medium temperature such that the Doppler broadening becomes comparable with the hyperfine splitting in the excited state, the peak transmittance drops down and finally disappears as shown in Fig. 4b and 4c. At the same time the three-level model predicts only a narrowing of the transparency window in agreement with Ref. [45]. This modification can be attributed to the six-level atoms which have Doppler shifts in the interval  $\Delta_D \in [20, 100]$  MHz. Some of them are not transparent for the probe field as we concluded from the previous section. From Fig. 3, it can be seen that the atoms moving in a direction opposite to the laser beam ( $\Delta_D > 0$ ) are at the origin of this effect.

Let us note that our study has focused on a regime where the control Rabi frequency is on the order of the excited state linewidth  $|\Omega_{e2s}^c| \sim \gamma$ . However, it can be shown that the strong reduction of the transparency will occur for smaller or larger frequencies. Figure 5 gives the transmittance of the medium for  $|\Omega_{e2s}^c| = 0.1\gamma$  and  $|\Omega_{e2s}^c| = 10\gamma$ . In both cases, large inhomogeneous broadening leads to the total disappearance of the transparency peak.

Experimentally, an EIT peak is still observed even at room temperature, but it is strongly reduced. As we

demonstrate in the next section, the non-zero value of the EIT signal, even if considerably degraded, is caused by some optical pumping to  $F = 4$  of the atoms that are not transparent to the probe field. This process was not taken into account in our theoretical model up to this point, but it will be treated in the next section.

This section demonstrated then that the EIT is strongly reduced in an inhomogeneously broadened ensemble of six-level atoms as compared to three-level atoms. The main reason has been clearly identified: it is the presence of the atoms with a particular Doppler shift that absorb the probe light while the others are nearly transparent. Based on this result, the following section investigates a scheme possibly enabling the improvement of the EIT in such systems.

## V. EIT ENHANCEMENT BY VELOCITY SELECTIVE OPTICAL PUMPING

The velocity classes of atoms leading to a strong reduction of the EIT have been clearly identified in the previous sections. In order to recover the transparency, these atoms should not participate in the process. In this section we discuss successively two optical pumping schemes that modify the velocity distribution in order to enhance the transparency.

### A. Optical pumping by the strong control field

Up to now we have considered a six-level system as a close approximation to the  $D_2$ -line of the cesium atom (Fig. 1). We have taken into account only one ground hyperfine sublevel  $F = 3$  which was coupled with the excited  $6^2P_{3/2}$  manifold by both control and probe fields. In this case the strong  $\sigma^+$  polarized control field optically pumps the atoms into state  $|g\rangle$ . However, during the optical pumping process the atom can spontaneously decay from the excited states to both ground hyperfine sublevels  $F = 3$  and  $F = 4$ . Taking the second hyperfine sublevel in the ground state into account leads to the fact that all atoms are eventually pumped to the  $F = 4$  state. Even atoms firstly pumped into state  $|g\rangle$  can be re-pumped via state  $|e\rangle$  to the upper ground state with  $F = 4$ . To bring back atoms in state  $|g\rangle$  a  $\sigma^+$  repumping polarized field resonant with the  $F = 4 \rightarrow F' = 4$  transition is applied. The repumping field (together with the control field), can bring a non-zero steady state population back into state  $|g\rangle$ .

Furthermore, the optical pumping process depends on the atomic velocity and can strongly modify the velocity distribution. To quantitatively estimate this effect we have simulated the entire optical pumping process and obtained a numerical steady state solution of the equations for the atomic density matrix using the following

interaction Hamiltonian:

$$V_{OP} = - \sum_{F=3}^4 \sum_{F'=F-1}^{F+1} \sum_{n=-F}^F \hbar \Omega_{F'n+1 F n} |F', n+1\rangle \langle F, n| + h.c. \quad (5.1)$$

Here the Rabi frequency  $\Omega_{F'n+1 F n}$  for the transition  $|F, n\rangle \rightarrow |F', n+1\rangle$  contains the control field amplitude if  $F = 3$  and the repump field amplitude if  $F = 4$ . Due to the complexity of the atomic level structure the full set of equations for the atomic density matrix is presented in Appendix B. Here we comment the main features of our optical pumping model and the results.

The efficiency of the optical pumping is limited by the relaxation processes. During the collisions with the cell walls the atomic spin as well as the velocity is changing. To model this process we introduce in our theory the decay of the ground state density matrix elements. The decay rate  $1/\tau_d$  is assumed to be much smaller than the excited state decay rate  $\gamma$ , so we can neglect the influence of the wall-collisions on the atom in the excited state. In our model, we assume that the randomisation times for the atomic velocity and for the atomic spin are equal, which can describe at least three experimental situations. First, when the cell walls do not have special coating preventing the spin relaxation and after one wall collision both atomic spin and velocity are randomly changed. Second, when the cell has a polarization preserving coating but the volume of the light beam is much smaller than the volume of the cell. In this case an atom will collide many times with the wall and thus randomly change its spin before coming back to the light beam. A third situation occurs when the optical pumping process reaches its steady state during the time it takes for an atom to cross the beam. In these cases, in order to find the steady state, we set  $\tau_d$  equal to the time of flight of the atom through the light beam.

In our calculations,  $\tau_d$  is chosen equal to  $300\mu s$ , which corresponds to an average time of flight of several centimeters for the cesium atoms at room temperature. The density of atoms was set to  $n_0 = 3.5 \times 10^{11} \text{ cm}^{-3}$ . This number is an order of magnitude larger than the one we used in the previous section, because here we consider the two ground states  $F = 3$  and  $F = 4$ .

We will keep the Rabi frequency of the control field to be the same as in the previous sections,  $\Omega_{e_{1s}}^c = 2\pi \times 12 \text{ MHz}$ . This corresponds, for example, to a control field power of 200 mW and a beam diameter equal to 1 cm. The repumping field is contra-propagating with respect to the control and probe fields, and its power is equal to 4.4 mW for a beam diameter of 1 cm.

Figure 6 gives the result of the optical pumping simulation. The velocity distribution of the atoms in state  $|g\rangle$  in the presence of the control and repumping beams is shown by the solid line. For comparison we also give the Gaussian distribution with a width  $\Gamma_D = 160 \text{ MHz}$  corresponding to room temperature  $T = 300 \text{ K}$ . We can see that the atoms propagating towards the con-

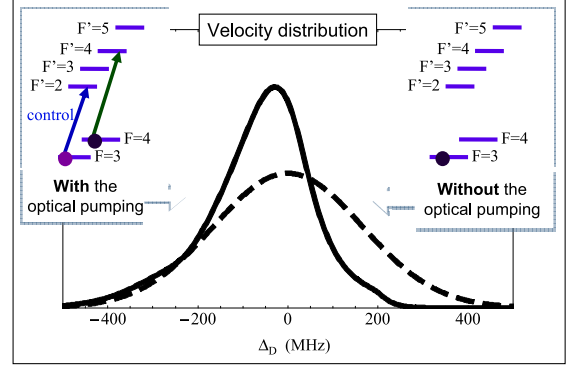


FIG. 6: (color online) Velocity distribution of the atoms in state  $|g\rangle$ . The distributions are normalized such as  $\int f(\Delta_D) d\Delta_D = 1$ . The dashed line represents the Gaussian distribution, assuming that all the atoms are prepared in state  $|g\rangle$  as shown in the right inset. The solid line shows the actual velocity distribution which can be achieved with the transfer of atoms due to optical pumping by the control field and the repumping field as shown in the left inset. The parameters are the following:  $\Omega_{e_{1s}}^c = 2.3\gamma = 2\pi \times 12 \text{ MHz}$ ,  $\Delta_c = 0$ , repumping power equal to 4.4 mW for a beam diameter of 1 cm,  $\tau_D = 300\mu s$ .

trol beam ( $\Delta_D > 0$ ) have been pumped out of state  $|g\rangle$ . This is due to the positive Doppler shift that brings the control light frequency closer to the atomic transition  $|F = 3\rangle \rightarrow |F' = 4\rangle$  and thus makes depopulation of the state  $|g\rangle$  more likely. As a consequence, the velocity distribution of atoms in state  $|g\rangle$  becomes narrower, indicating an effective cooling mechanism.

According to the conclusion of section III, atoms with positive Doppler shifts are the ones which previously contributed to the disappearance of the EIT. Due to the optical pumping process, these atoms, which move in the opposite direction to the probe and control beams, are partially removed from the interaction process. Using the new velocity distribution in the calculations we can see how it helps to recover the transparency. In Fig. 7, we show the transmittance of a cesium vapor calculated including the optical pumping effect. Contrary to the case of a Gaussian velocity distribution, in which the EIT resonance vanishes, a transparency peak is obtained with the modified velocity distribution. In [15], EIT was indeed experimentally observed on the  $D_2$  line of Cs, while the combined effect of broadening and multi-level structure should lead to a fully vanishing of the EIT.

We have thus demonstrated that the effective cooling due to the optical pumping process by the control field allows to observe the EIT effect in the configuration presented in Fig. 1.

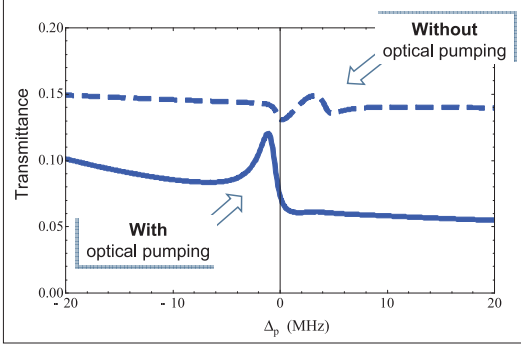


FIG. 7: (color online) Transmittance for the probe field with and without optical pumping. The dashed curve corresponds to six-level atoms in state  $|g\rangle$  having a Gaussian velocity distribution. The EIT peak vanishes in these conditions as shown in the previous section. The solid line shows the transmittance when the velocity distribution is modified by the optical pumping due to the control and the repumping fields. The EIT peak is partly recovered since part of the absorbing atoms are pumped out to sublevel  $F = 4$  and thus do not interact any more with the probe field. The parameters are the same as for Fig. 6

### B. Hole burning in the velocity distribution

Based on the previous result, we now present a procedure that allows to further enhance the EIT contrast without changing the medium optical depth. The main idea is to burn a hole in the velocity distribution of atoms in state  $|g\rangle$ . Thus we exclude atoms with a specific Doppler shift from the interaction process.

In addition to the control, probe and repumping fields discussed in the previous subsection, one more  $\sigma^+$  polarized pump field is used. It is detuned by  $\Delta_{pump}$  from the transition between  $F = 3$  and  $F' = 4$  sub-levels. It will then pump the atoms with a Doppler shift  $\Delta_D = -\Delta_{pump}$  out of the  $F = 3$  level, thus creating a hole in the velocity distribution. We simulate this additional optical pumping process by introducing an effective depopulation rate  $\gamma_{pump}$  for the atoms in state  $|F = 3, m_F = 3\rangle$ :

$$\gamma_{pump}(\Delta_D) = \frac{\gamma \Omega_{pump}^2}{4(\Delta_D + \Delta_{pump})^2 + \gamma^2 + \Omega_{pump}^2} \quad (5.2)$$

where  $\Omega_{pump}$  is the Rabi frequency of the pump field with respect to the transition  $|g\rangle \leftrightarrow |e\rangle$ . The structure of this expression shows a Lorentzian dependence with the Doppler shift. The width of this Lorentzian curve, which gives the width of the dip on the velocity distribution, depends in the Rabi frequency of the field but it is never smaller than the natural linewidth of the atomic excited state  $\gamma$ .

Figure 8 shows the velocity distribution of atoms in state  $|g\rangle$  and the resulting transmittance for the probe.

We examine the cases of different values of the pump field detuning  $\Delta_{pump}$ , keeping the pump Rabi frequency equal to  $\Omega_{pump} = 0.15\gamma$ . Comparing the cases of negative and positive detunings, we see that the EIT enhancement is larger when the pump detuning is negative. This is due to the fact that atoms with positive Doppler shifts, pumped out of the interaction process in this case, contribute more to the absorption than atoms with negative Doppler shifts as shown in Fig. 3(b). We see that the EIT enhancement is the largest when  $\Delta_{pump} = -40$  MHz. We should also note that the EIT contrast grows when the pump Rabi frequency is increased because more absorbing atoms are depumped and thus removed from the interaction process.

This result confirms our interpretation of the EIT formation in a Doppler broadened  $D$ -line of the alkali-metal atoms. One can define the EIT contrast as  $C \equiv (t_{max} - t_{min}) / (1 - t_{min})$ , where  $t_{max}$  is the probe transmittance in the maximum of the EIT peak and  $t_{min}$  is the probe transmittance on the plateau, which defines the optical depth of the medium on the side of the EIT resonance. It can be seen in Fig. 8 that our scheme provides an enhancement of this contrast by approximately 8 times.

## VI. CONCLUSION

Our analysis demonstrates the influence of multiple excited levels on EIT in alkali-metal atoms. We have shown that the presence of more than one excited state in the  $\Lambda$ -type interaction can lead to a significant change as compared with the three-level approximation. This change is small when the inhomogeneous broadening is much smaller than the separation between the excited states. However, even for cold atoms, it leads to a noticeable decrease in transparency.

The effect becomes large when the broadening is comparable with the separation between the excited states, which may lead to the total disappearance of the transparency. This effect of the multilevel structure is caused by two reasons. The first one is the ac-Stark shift of the atomic dressed states, which varies with the Doppler shift. In a multilevel atom this variation leads to having no probe-field frequency for which atoms from all the velocity classes are transparent. The second reason is the interference between several  $\Lambda$  transitions appearing when both fields are tuned between the hyperfine transitions, increasing the off-resonant Raman scattering cross section.

After explaining the origin of the EIT suppression in a Doppler broadened medium, in particular by clearly identifying the atoms which strongly absorb the probe, we have proposed a method to enhance the transparency. It is based on an effective cooling mechanism using optical pumping. In particular, by creating a dip in the velocity distribution of atoms participating in the interaction process we achieve a significant enhancement of the EIT

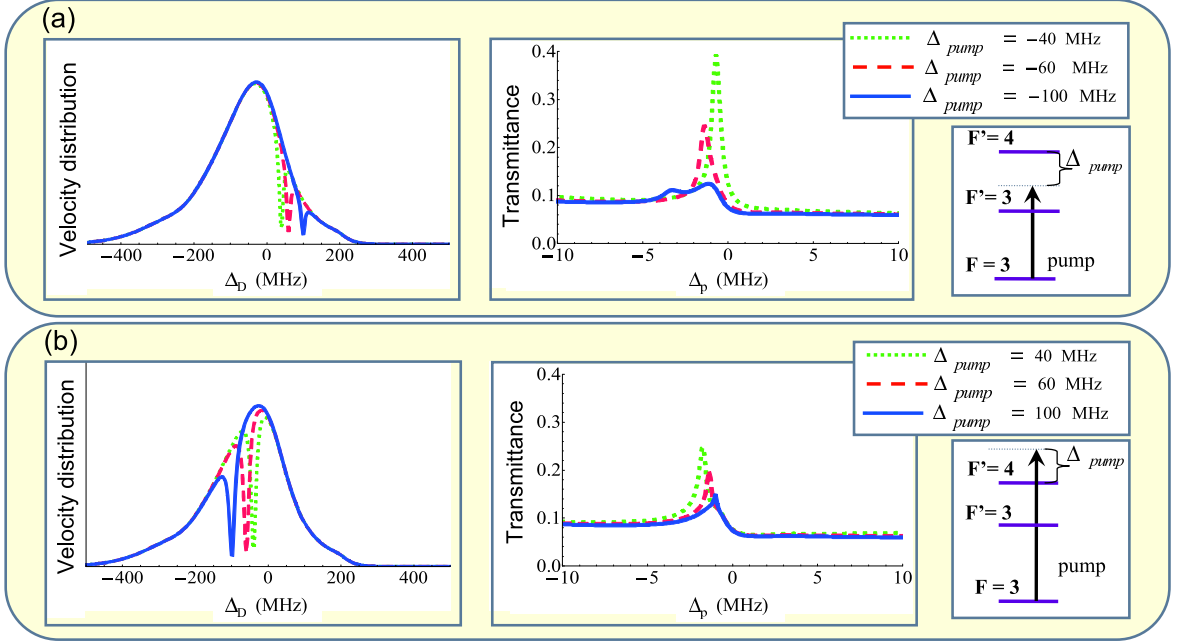


FIG. 8: (color online) Influence of the additional pump on the velocity distribution of atoms in state  $|g\rangle$  (1st column) and on the probe field transparency (2nd column). The optical pumping leads to a hole burning effect in the velocity distribution, which results in an enhancement of the EIT. Different probe field detunings are presented with  $\Delta_{pump} < 0$  in the upper panel and  $\Delta_{pump} > 0$  in the lower panel. The Rabi frequency of the pump field with respect to the transition between  $|g\rangle$  and  $|e\rangle$  sublevels remains constant  $\Omega_{pump} = 0.15\gamma$ . Calculations are done in the same conditions for the control and repumping fields as in Fig. 6:  $\Omega_{e1s}^c = 2.3\gamma = 2\pi \times 12$  MHz,  $\Delta_c = 0$ , repumping power equal to 4.4 mW for a beam diameter of 1 cm,  $\tau_D = 300\mu s$ .

contrast. This technique is expected to allow improvements in current experimental realizations of EIT-based quantum memories in room temperature alkali-metal vapors. Our analysis might also be relevant for other coherent effects in such vapors, like in the recent entangled light generation by four-wave mixing [49, 50].

### Acknowledgments

We thank Igor Sokolov and Alberto Amo for fruitful discussions. This work is supported by the EC under the ICT/FET project COMPAS, by the RFBR (Grants No. 10-02-00103), and by the CAPES/COFECUB project QE-COMET. O. Mishina acknowledges the financial support from the Ile-de-France programme IFRAF and A. Sheremet from the Foundation "Dynasty".

### Appendix A

In this appendix we present the details of the susceptibility calculations for the six-level system presented in Fig. 1. In section II only a part of the results related

to the multi- $\Lambda$  system is discussed. Here we will follow the derivation and then discuss the full solution in more details.

First we introduce a set of slowly varying operators for the off-diagonal elements of the atomic density matrix:

$$\begin{aligned}
 \sigma_{e_{F'}g} &= \rho_{e_{F'}g} e^{i\omega_p t} \\
 \sigma_{sg} &= \rho_{sg} e^{i(\omega_p - \omega_c)t} \\
 \sigma_{ge} &= \rho_{ge} e^{i(-\omega_c)t} \\
 \sigma_{se} &= \rho_{se} e^{i(\omega_p - 2\omega_c)t} \\
 \sigma_{e_{F'}e} &= \rho_{e_{F'}e} e^{i(\omega_p - \omega_c)t}
 \end{aligned} \tag{A1}$$

where  $F' = 2, 3, 4$  refer to the excited states with different angular momenta. In addition to the earlier introduced optical coherences  $\sigma_{e_{F'}g}$  on the probe field transition (2.4), (A1) includes as well the coherence between the ground states  $\sigma_{sg}$ , the optical coherence  $\sigma_{ge}$  on the  $|g\rangle$  to  $|e\rangle$  transition, the coherence  $\sigma_{se}$  caused by the three-photon transition  $|s\rangle \rightarrow |e_{F'}\rangle \rightarrow |g\rangle \rightarrow |e\rangle$ , and the coherences  $\sigma_{e_{F'}e}$  between excited states  $|e\rangle$  and  $|e_{F'}\rangle$ .

Now we present the subsequent solution of the density matrix equations (2.6). First we consider the zero order



equations taking into account only the control field:

$$\begin{aligned}
\dot{\rho}_{ss}^{(0)} &= -\tau_d^{-1} \rho_{ss}^{(0)} + \tau_d^{-1}/2 + \gamma/2 \sum_{F'} \rho_{e_{F'}e_{F'}}^{(0)} \\
&\quad - i \sum_{F'} (\sigma_{se_{F'}}^{(0)} \Omega_{e_{F'}s}^c - \sigma_{e_{F'}s}^{(0)} \Omega_{se_{F'}}^c)/2 \\
\dot{\rho}_{gg}^{(0)} &= -\tau_d^{-1} \rho_{gg}^{(0)} + \tau_d^{-1}/2 + \gamma/2 \sum_{F'} \rho_{e_{F'}e_{F'}}^{(0)} + \gamma \rho_{ee}^{(0)} \\
&\quad - i(\sigma_{ge}^{(0)} \Omega_{eg}^c - \sigma_{eg}^{(0)} \Omega_{ge}^c)/2 \\
\dot{\rho}_{e_{F'_1}e_{F'_2}}^{(0)} &= -(i\omega_{e_{F'_1}e_{F'_2}} + \gamma) \rho_{e_{F'_1}e_{F'_2}}^{(0)} \\
&\quad - i(\rho_{e_{F'_1}s}^{(0)} \Omega_{se_{F'_2}}^c - \rho_{se_{F'_2}}^{(0)} \Omega_{e_{F'_1}s}^c)/2 \quad (\text{A2}) \\
\dot{\sigma}_{eg}^{(0)} &= (i\Delta_c - i\omega_{ee_2} - \frac{\gamma}{2}) \sigma_{eg}^{(0)} + i(\rho_{gg}^{(0)} - \rho_{ee}^{(0)}) \frac{\Omega_{eg}^c}{2} \\
\dot{\sigma}_{e_{F'}s}^{(0)} &= (i\Delta_c - i\omega_{e_{F'}e_2} - \frac{\gamma}{2}) \sigma_{e_{F'}s}^{(0)} \\
&\quad + i\rho_{ss}^{(0)} \frac{\Omega_{e_{F'}s}^c}{2} - i \sum_{F'_1} \rho_{e_{F'}e_{F'_1}}^{(0)} \frac{\Omega_{e_{F'_1}s}^c}{2} \quad (\text{A3})
\end{aligned}$$

Here notations are the same as in Sec. II: the Rabi frequencies are  $\Omega_{e_{F'}s}^c = 2d_{e_{F'}s}\varepsilon_c/\hbar$ ,  $\Omega_{eg}^c = 2d_{eg}\varepsilon_c/\hbar$ ,  $\Omega_{e_{F'}g}^p = 2d_{e_{F'}g}\varepsilon_p/\hbar$  and the transition energies are  $\omega_{ij} = (E_i - E_j)/\hbar$ , where  $E_i$  is the energy of the unperturbed atomic state  $|i\rangle$ . Indexes  $F'$  and  $F'_1$  run through the values 2, 3 and 4.

Decay mechanisms included in our equations model an excited state radiative decay with the rate  $\gamma$  and a ground state decay due to the finite time of flight  $\tau_d$  of the atoms through the light beam. We assume that the loss rate of atoms is much smaller than the radiative decay rate  $\tau_d^{-1} \ll \gamma$ . For our calculations we consider a vapor of cesium atoms. The radiative decay is then  $\gamma^{-1} = 30$  ns, and we assume  $\tau_d = 300 \mu\text{s}$ , corresponding to the time of flight at room temperature through a light beam of few centimeters in diameter. We assume that at the

same rate as atoms are leaving the beam, new unpolarized atoms will be entering the interaction region. This is included by the source term  $+\tau_d^{-1}/2$  in equations (A2).

Throughout the article we use the conditions that all Rabi frequencies are much smaller than the hyperfine splittings  $\Omega_{e_{F'}s}^c \ll \omega_{e_{F'}e_2}$ . In this case we neglect the coherences  $\rho_{e_{F'_1}e_{F'_2}}^{(0)}$  between different excited states  $F'_1 \neq F'_2$ , which brings us to the following stationary solutions:

$$\begin{aligned}
\rho_{ss}^{(0)} &= \frac{1}{2} \left( 1 + \tau_d \sum_{F'} \frac{|\Omega_{e_{F'}s}^c|^2 \gamma/2}{4(\Delta_c - \omega_{ee_2})^2 + \gamma^2 + |\Omega_{e_{F'}s}^c|^2} \right)^{-1} \\
\rho_{gg}^{(0)} &= \frac{1}{2} + \tau_d \rho_{ss}^{(0)} \sum_{F'} \frac{|\Omega_{e_{F'}s}^c|^2 \gamma/2}{4(\Delta_c - \omega_{ee_2})^2 + \gamma^2 + |\Omega_{e_{F'}s}^c|^2} \\
\sigma_{ge}^{(0)} &= \frac{2(\Delta_c - \omega_{ee_2} - i\gamma/2) \Omega_{ge}^c}{4(\Delta_c - \omega_{ee_2})^2 + \gamma^2 + |\Omega_{eg}^c|^2} \rho_{gg}^{(0)} \quad (\text{A4})
\end{aligned}$$

Using the solution (A4) it can be verified that atoms from all the velocity classes are pumped from the state  $|s\rangle$  to the state  $|g\rangle$  with a high efficiency. Note that in this six-level model all the atoms are eventually pumped to state  $|g\rangle$ . Experimentally the presence of the other hyperfine ground state with  $F = 4$  will affect considerably the atomic population in state  $|g\rangle$  which justifies the approximation  $\rho_{gg}^{(0)} \sim 1$  made in Sec. II. Atoms from this state  $|g\rangle$  may be pumped to the state with  $F = 4$ , which will render them transparent for the control and probe fields. This process represents an important limitation for the maximum optical depth that can be achieved in the configuration of Fig. 1. In Sec. V and Appendix B this optical pumping mechanism will be taken fully into account. Here we do not consider it for simplicity and to clarify the influence of the excited hyperfine structure on the EIT signal.

Now we proceed further along Eqs. (2.6) towards the first order equation with respect to the weak probe field:

$$\begin{aligned}
\frac{d\sigma_{e_{F'}g}^{(1)}}{dt} &= (i\Delta_p - i\omega_{e_{F'}e_2} - \gamma_{e_{F'}g}) \sigma_{e_{F'}g}^{(1)} + i(\rho_{gg}^{(0)} \Omega_{e_{F'}g}^p + \sigma_{sg}^{(1)} \Omega_{e_{F'}s}^c - \sigma_{e_{F'}e}^{(1)} \Omega_{eg}^c)/2 \\
\frac{d\sigma_{sg}^{(1)}}{dt} &= (i\Delta_p - i\Delta_c - \gamma_{sg}) \sigma_{sg}^{(1)} - i\sigma_{se}^{(1)} \Omega_{eg}^c/2 + i \sum_{F'=2}^4 \sigma_{e_{F'}g}^{(1)} \Omega_{se_{F'}}^c/2 \\
\frac{d\sigma_{se}^{(1)}}{dt} &= (i\Delta_p - 2i\Delta_c + i\omega_{sg} + i\omega_{ee_2} - \gamma_{se}) \sigma_{se}^{(1)} - i\sigma_{sg}^{(1)} \Omega_{ge}^c/2 + i \sum_{F'=2}^4 \sigma_{e_{F'}e}^{(1)} \Omega_{se_{F'}}^c/2 \\
\frac{d\sigma_{e_{F'}e}^{(1)}}{dt} &= (i\Delta_p - i\Delta_c + i\omega_{e_{F'}e} + i\omega_{sg} - \gamma_{e_{F'}e}) \sigma_{e_{F'}e}^{(1)} + i(\sigma_{ge}^{(0)} \Omega_{e_{F'}g}^p - \sigma_{e_{F'}e}^{(1)} \Omega_{ge}^c + \sigma_{se}^{(1)} \Omega_{e_{F'}s}^c)/2 \quad (\text{A5})
\end{aligned}$$

From Eqs. (A5) we find the steady state solution for the

optical and ground state coherences

$$\begin{aligned}
\sigma_{sg}^{(1)} &= \rho_{gg}^{(0)} \sum_{F'} \frac{\Omega_{se_{F'}}^c}{2\Delta_{sg}} \left[ \frac{\Omega_{e_{F'}g}^p}{2\Delta_{e_{F'}g}} + \frac{\varepsilon_p |\Omega_{eg}^c|^2 T_{F'}}{4\hbar \Delta_{e_{F'}e} \Delta_{e_{F'}g}} \right] \\
&\quad + \sigma_{ge}^{(0)} \sum_{F'} \frac{\varepsilon_p \Omega_{eg}^c \Omega_{se_{F'}}^c}{4\hbar \Delta_{e_{F'}e} \Delta_{sg}} \left( H'_{F'} + \frac{d_{e_{F'}g}}{\Delta_{se}} \right) \quad (\text{A6})
\end{aligned}$$

$$\begin{aligned}
\sigma_{e_{F'}g}^{(1)} = & -\rho_{gg}^{(0)} \left[ \frac{\Omega_{e_{F'}g}^p}{2\Delta_{e_{F'}g}} + \frac{|\Omega_{eg}^c|^2}{4\Delta_{e_{F'}e}\Delta_{e_{F'}g}} \frac{\varepsilon_p}{\hbar} D'_{F'} \right] \\
& -\sigma_{sg}^{(1)} \left[ \frac{\Omega_{e_{F'}s}^c}{2\Delta_{e_{F'}g}} + \frac{|\Omega_{eg}^c|^2}{4\Delta_{e_{F'}e}\Delta_{e_{F'}g}} G'_{F'} \right] \\
& -\sigma_{ge}^{(0)} \frac{\Omega_{eg}^c}{2\Delta_{e_{F'}e}} \frac{\varepsilon_p}{\hbar} H'_{F'} \quad (A7)
\end{aligned}$$

The denominators  $\Delta_{e_{F'}g}$ ,  $\Delta_{e_{F'}e}$ ,  $\Delta_{se}$  and  $\Delta_{sg}$  are presented in expression (2.10).

In order to clarify the structure of Eqs. (A6,A7), we have grouped its terms to highlight the different interaction schemes. The terms proportional to  $\rho_{gg}^{(0)}$  with all components written explicitly are related  $\Lambda$ -type interactions via the various excited levels  $F'$ . This part will be dominant under the conditions we discuss in this paper, i.e., the control field far detuned from the  $|g\rangle$  to  $|e\rangle$  transition. The other terms of Eqs. (A6,A7) are given as a function of the coefficients  $D'_{F'}$ ,  $G'_{F'}$ ,  $T'_{F'}$ , and  $H'_{F'}$ , which have the following form:

$$\begin{aligned}
G'_{F'} &= \frac{\Omega_{e_{F'}s}^c}{2\Delta_{e_{F'}g}} + \frac{\Omega_{e_{F'}s}^c}{2\Delta_{se}} \left( 1 + \sum_{F'_1} \frac{|\Omega_{se_{F'_1}}^c|^2}{4\Delta_{e_{F'_1}e}\Delta_{e_{F'_1}g}} \right) \\
H'_{F'} &= \frac{d_{e_{F'}g}}{\Delta_{e_{F'}g}} + \frac{\Omega_{e_{F'}s}^c}{\Delta_{e_{F'}g}\Delta_{se}} \sum_{F'_1} \frac{\Omega_{se_{F'_1}}^c d_{e_{F'_1}g}}{4\Delta_{e_{F'_1}e}} \\
T'_{F'} &= \frac{d_{e_{F'}g}}{\Delta_{e_{F'}g}} + \frac{d_{e_{F'}g}}{\Delta_{se}} + \frac{\Omega_{e_{F'}s}^c}{4\Delta_{se}} \sum_{F'_1} \frac{\Omega_{se_{F'_1}}^c d_{e_{F'_1}g}}{\Delta_{e_{F'_1}e}\Delta_{e_{F'_1}g}} \\
D'_{F'} &= \frac{d_{e_{F'}g}}{\Delta_{e_{F'}g}} + \frac{\Omega_{e_{F'}s}^c}{4\Delta_{se}} \sum_{F'_1} \frac{\Omega_{se_{F'_1}}^c d_{e_{F'_1}g}}{\Delta_{e_{F'_1}e}\Delta_{e_{F'_1}g}} \quad (A8)
\end{aligned}$$

These coefficients represent the parts of the Eqs. (A6,A7) related to the processes involving the  $|g\rangle$  to  $|e\rangle$  transition. They describe then  $V$ -type and  $N$ -type processes. In the present article we are mainly focused on the  $\Lambda$ -type interactions, which play the dominant role under the chosen conditions. For this reason, in the main text we do not present explicitly the terms of Eqs. (2.9,2.10,2.11) related to such  $V$ -type and  $N$ -type processes. Instead we introduce the coefficients  $N_{e_{F'}g}$  and  $\Delta_N$ :

$$\begin{aligned}
N_{e_{F'}g} &= \frac{|\Omega_{eg}^c|^2}{4\Delta_{e_{F'}g}} \left( \frac{D'_{F'}}{\Delta_{e_{F'}e}} + \frac{\Omega_{e_{F'}s}^c}{4\Delta_{sg}} \sum_{F'_1} \frac{\Omega_{se_{F'_1}}^c T'_{F'_1}}{\Delta_{e_{F'_1}e}\Delta_{e_{F'_1}g}} \right) \\
&+ \frac{|\Omega_{eg}^c|^2 G'_{F'}}{\Delta_{e_{F'}e}\Delta_{e_{F'}g}} \sum_{F'_1} \frac{\Omega_{se_{F'_1}}^c \left( d_{e_{F'_1}g} + \frac{|\Omega_{eg}^c|^2 T'_{F'_1}}{4\Delta_{e_{F'_1}e}} \right)}{8\Delta_{sg}\Delta_{e_{F'_1}g}} \\
\Delta_N &= \sum_{F'} \frac{|\Omega_{eg}^c|^2 \Omega_{se_{F'}}^c}{2\Delta_{e_{F'}e}\Delta_{e_{F'}g}} \left( G'_{F'} + \frac{\Omega_{e_{F'}s}^c}{2\Delta_{se}} \right). \quad (A9)
\end{aligned}$$

## Appendix B

In this appendix we present the complete set of equations describing the optical pumping process discussed in sec. IV.

We begin with the case where a  $\sigma^+$  polarized repump field and a  $\sigma^+$  control field resonant to the atomic transitions  $|F=4\rangle$  to  $|F'=4\rangle$  and  $|F=3\rangle$  to  $|F'=2\rangle$  respectively as described in sec. V A. Based on the interaction Hamiltonian 5.1 we derive the following system of equations:

$$\begin{aligned}
\frac{d\rho_{F_a n F_b n}(\Delta_D)}{dt} &= (i\omega_{F_b F_a} - \frac{1}{\tau_d})\rho_{F_a n F_b n} + \frac{\delta_{F_a F_b}}{\tau_d} \frac{f^0(\Delta_D)}{(2S+1)(2I+1)} + \delta_{F_a F_b} \gamma \sum_{\substack{F_a-1 \leq F' \leq F_a+1 \\ n-1 \leq k \leq n+1}} P_{|F',k\rangle \rightarrow |F_a,n\rangle} \rho_{F'k F'n} \\
&+ i \sum_{F'_1, F'_2} \left[ \frac{\Omega_{F'_1 n+1 F_b n} \Omega_{F'_2 n+1 F_a n}}{4\Delta_{F'_1 F_a}} \rho_{F'_2 n+1 F'_1 n+1} + \frac{\Omega_{F'_1 n+1 F_a n} \Omega_{F'_2 n+1 F_b n}}{4\Delta_{F'_1 F_b}^*} \rho_{F'_1 n+1 F'_2 n+1} \right] \\
&- i \sum_{F'_1, F_1} \left[ \frac{\Omega_{F'_1 n+1 F_b n} \Omega_{F'_1 n+1 F_1 n}}{4\Delta_{F'_1 F_a}} \rho_{F_a n F_1 n} + \frac{\Omega_{F'_1 n+1 F_a n} \Omega_{F'_1 n+1 F_1 n}}{4\Delta_{F'_1 F_b}^*} \rho_{F_1 n F_b n} \right] \\
\frac{d\rho_{F'_a n F'_b n}(\Delta_D)}{dt} &= (i\omega_{F'_b F'_a} - \gamma)\rho_{F'_a n F'_b n} - i \sum_{F'_1, F_1} \left[ \frac{\Omega_{F'_b n F_1 n-1} \Omega_{F'_1 n F_1 n-1}}{4\Delta_{F'_a F_1}^*} \rho_{F'_a n F'_1 n} + \frac{\Omega_{F'_a n F_1 n-1} \Omega_{F'_1 n F_1 n-1}}{4\Delta_{F'_b F_1}^*} \rho_{F'_1 n F'_b n} \right] \\
&+ i \sum_{F_1, F_2} \left[ \frac{\Omega_{F'_b n F_1 n-1} \Omega_{F'_a n F_2 n-1}}{4\Delta_{F'_a F_1}^*} \rho_{F_2 n-1 F_1 n-1} + \frac{\Omega_{F'_a n F_1 n-1} \Omega_{F'_b n F_2 n-1}}{4\Delta_{F'_b F_1}^*} \rho_{F_1 n-1 F_2 n-1} \right] \quad (B1)
\end{aligned}$$

To obtain this system we adiabatically eliminate the optical coherences  $\rho_{F'_b n+1 F_a n}(\Delta_D) \equiv \langle F'_b, n+1 | \rho(\Delta_D) | F_a, n \rangle$

from the full system of equations. The first equation represents the evolution of the ground state de-

scribed by the density matrix elements  $\rho_{F_a n F_b n}(\Delta_D) \equiv \langle F_a, n | \rho(\Delta_D) | F_b, n \rangle$ . The total angular momentum of the alkali-metal in the ground state can have two different values  $I \pm 1/2$ , in case of the  $^{133}\text{Cs}$  they will be  $F_a, F_b = 3, 4$ . The second term on the right side of the first equation describes the source of atoms in the initial state entering the interaction volume with a rate equal to the loss rate  $1/\tau_d$ . The initial population is equally distributed among the Zeeman sublevels of the ground states with the probability  $f^0(\Delta_D)/(2S+1)/(2I+1)$  given by the initial Gaussian velocity distribution  $f^0(\Delta_D) = (2\pi\Gamma_D^2)^{-1/2} \exp(-\Delta_D^2/2\Gamma_D^2)$  divided by the number of available ground states. By  $\delta_{ij}$  we define the Kronecker symbol. The last term in the first line describes the radiative decay from different excited states  $|F', k\rangle$  with  $k = n-1, n, n+1$  to the ground state  $|F_a, n\rangle$  with the rate  $\gamma \cdot p_{|F', k\rangle \rightarrow |F, n\rangle}$  given by the value of the reduced dipole moment of the transition  $|F', k\rangle \rightarrow |F, n\rangle$  [48]:

$$p_{|F', k\rangle \rightarrow |F, n\rangle} = (2J+1)(2F+1) \left[ C_{F n 1 k-n}^{F' k} \right]^2 \left\{ \begin{matrix} \frac{1}{2} & I & F \\ F' & 1 & J \end{matrix} \right\}^2 \quad (\text{B2})$$

The Clebsh-Gordan coefficient  $C_{F n 1 k-n}^{F' k}$  and the 6j-symbol  $\left\{ \begin{matrix} \frac{1}{2} & I & F \\ F' & 1 & J \end{matrix} \right\}$  give the transition properties resulting in  $\sum_{k=n-1}^{n+1} p_{|F', k\rangle \rightarrow |F, n\rangle} = 1$ . The last two double sums in the first equation show the Hamiltonian dynamic in the presence of two fields with Rabi frequencies  $\Omega_{F'_b F_a n-1}$  which contain the amplitude of the control field if  $F_a = 3$  or the amplitude of the repumping field if  $F_a = 4$ . The denominators in these terms are equal to  $\Delta_{F'_b F_a} \equiv i\frac{\gamma}{2} - \Delta_{F'_b F_a} - \Delta_D$ . Summation over the hyperfine levels in these terms goes from  $I-S-L$  to  $I+S+L$  where  $S = 1/2$  and  $L = 0$  in case of the ground states and  $L = 1$  in case of the excited states.

The second equation in the system (B1) describes the evolution of the excited state given by the density matrix elements  $\rho_{F'_a n F'_b n}(\Delta_D) \equiv \langle F'_a, n | \rho(\Delta_D) | F'_b, n \rangle$ . In

the  $D_2$ -line of the alkali-metal atom, the total angular momentum of the excited state can have four different values, in case of the  $^{133}\text{Cs}$  they will be  $F'_a, F'_b = 2, 3, 4, 5$ . This equation has a structure which is similar to the first one, except three major differences: the relaxation rate is given by the natural decay rate  $\gamma$ , much larger than  $1/\tau_d$ ; the initial population of the excited state is zero; and there are no source terms due to the decay from the other states.

Solving numerically equations (B1) we obtain the velocity distribution of atoms in state  $|g\rangle \equiv |F = 3, m_F = 3\rangle$  modified by the optical pumping process  $f(\Delta_D) \sim \rho_{gg}(\Delta_D)$ . It is presented in Fig. 6 (solid line) and used for the calculation of the transmittance in Fig. 7 (solid line).

As proposed in sec. VB an additional  $\sigma^+$  polarized "pump" field detuned by  $\Delta_{pump}$  from the transition  $|F = 3\rangle \leftrightarrow |F' = 4\rangle$  can be used to enhance the EIT contrast. The atoms with a Doppler shift  $\Delta_D = -\Delta_{pump}$  would be transferred from the state  $|g\rangle$  to the state  $|F = 3, m_F = 3\rangle \equiv |g_3\rangle$  or  $|F = 4, m_F = 4\rangle \equiv |g_4\rangle$  due to a resonant optical pumping process via the excited state  $|e\rangle \equiv |F' = 4, m_{F'} = 4\rangle$ . To simulate this process, we add the following terms to the right side of the first equation of the system (B1)

$$\begin{aligned} & -\gamma_{pump}(1 - p_{|e\rangle \rightarrow |g\rangle})\delta_{F_a 3}\delta_{n 3}\rho_{F_a n F_a n} \\ & +\gamma_{pump}p_{|e\rangle \rightarrow |g_3\rangle}\delta_{F_a 4}\delta_{n 3}\rho_{F_a n F_a n} \\ & +\gamma_{pump}p_{|e\rangle \rightarrow |g_4\rangle}\delta_{F_a 4}\delta_{n 4}\rho_{F_a n F_a n}. \end{aligned} \quad (\text{B3})$$

Here  $\gamma_{pump}$  is an effective depopulation rate, given by expression (5.2), and that depend on  $\Omega_{pump}$ , the Rabi frequency of the pump field with respect to the transition  $|g\rangle \leftrightarrow |e\rangle$ . Relative transition rates  $p_{|e\rangle \rightarrow |g\rangle}$ ,  $p_{|e\rangle \rightarrow |g_3\rangle}$  and  $p_{|e\rangle \rightarrow |g_4\rangle}$  take into account three allowed transitions for the atomic decay from state  $|e\rangle$  to the states  $|g\rangle$ ,  $|g_3\rangle$  or  $|g_4\rangle$  respectively. They can be found from expression (B2) and in case of the cesium atom  $p_{e \rightarrow g} = 25/60$ ,  $p_{e \rightarrow g_3} = 7/60$  and  $p_{e \rightarrow g_4} = 28/60$ .

---

[1] S.E. Harris, J.E. Field, and A. Imamoglu, Phys. Rev. Lett. **64**, 1107 (1990).  
[2] K.-J. Boller, A. Imamoglu, and S.E. Harris, Phys. Rev. Lett. **66**, 2593 (1991).  
[3] S.E. Harris, Phys. Today **50**, 36 (1997).  
[4] L.V. Hau, S.E. Harris, Z. Dutton, and C.H. Behroozi, Nature **397**, 594 (1999).  
[5] C. Liu, Z. Dutton, C.H. Behroozi, and L.V. Hau, Nature **409**, 490 (2001).  
[6] D.F. Phillips, A. Fleischhauer, A. Mair, R.L. Walsworth, and M.D. Lukin, Phys. Rev. Lett. **86**, 783 (2001).  
[7] H.J. Kimble, Nature **453**, 1023 (2008).  
[8] A.I. Lvovsky, B.C. Sanders, and W. Tittel, Nature Photon. **3**, 706 (2009).  
[9] N. Sangouard, C. Simon, H. de Riedmatten, and N.

Gisin, arXiv:0906.2699  
[10] D.N. Matsukevich, S.D. Jenkins, S. Lan, T.A.B. Kennedy, and A. Kuzmich, Nature **438**, 833 (2005).  
[11] M.D. Eisaman, A. Andre, F. Massou, M. Fleischhauer, A.S. Zibrov, and M.D. Lukin, Nature **438**, 837 (2005).  
[12] K.S. Choi, H. Deng, J. Laurat, and H.J. Kimble, Nature **452**, 67 (2008).  
[13] K. Honda, D. Akamatsu, M. Arikawa, Y. Yokoi, K. Akiba, S. Nagatsuka, T. Tanimura, A. Furusawa, and M. Kozuma, Phys. Rev. Lett. **100**, 093601 (2008).  
[14] J. Appel, E. Figueroa, D. Korystov, M. Lobino, and A.I. Lvovsky, Phys. Rev. Lett. **100**, 093602 (2008).  
[15] J. Cviklinski, J. Ortalo, J. Laurat, A. Bramati, M. Pinard, and E. Giacobino, Phys. Rev. Lett. **101**, 133601 (2008).

- [16] J. Ortalo, J. Cviklinski, P. Lombardi, J. Laurat, A. Bramati, M. Pinard, and E. Giacobino, *J. Phys. B* **42**, 114010 (2009).
- [17] M. Fleischhauer and J.P. Marangos, *Rev. Mod. Phys.* **77**, 633 (2005).
- [18] K. Hammerer, A.S. Sørensen, and E.S. Polzik, *Rev. Mod. Phys.* **82**, 1041 (2010).
- [19] K. Li, L. Deng, and M.G. Payne, *Appl. Phys. Lett.* **95**, 221103 (2009).
- [20] E. Cerboneschi and E. Arimondo, *Phys. Rev. A* **54**, 5400 (1996).
- [21] E.A. Korsunsky and D. V. Kosachiov, *Phys. Rev. A* **60**, 4996 (1999).
- [22] Q. Glorieux, R. Dubessy, S. Guibal, L. Guidoni, J.P. Likforman, T. Coudreau, E. Arimondo, *arXiv:1007.1610v2* (2010).
- [23] Z. Deng, *Opt. Commun.* **48**, 8 (1983).
- [24] H. Xia, S.J. Sharpe, A.J. Merriam, and S. E. Harris, *Phys. Rev. A* **56**, R3362 (1997).
- [25] O.S. Mishina, D.V. Kupriyanov, J.H. Müller, and E.S. Polzik, *Phys. Rev. A* **75**, 042326 (2007).
- [26] O.S. Mishina, A.S. Sheremet, N.V. Larionov, and D.V. Kupriyanov, *Optics and Spectroscopy* **108**, 313 (2010).
- [27] A.S. Sheremet, L.V. Gerasimov, I.M. Sokolov, D.V. Kupriyanov, O.S. Mishina, E. Giacobino, J. Laurat, *Phys. Rev. A* **82**, 033838 (2010).
- [28] J. Bateman, A. Xuereb, T. Freearde, *Phys. Rev. A* **81**, 043808 (2010).
- [29] D. Bhattacharyya, B. Ray, and P.N. Ghosh, *J. Phys. B* **40**, 4061 (2007).
- [30] Y. Chen, X.G. Wei, and B.S. Ham, *Opt. Express* **17**, 1781 (2009).
- [31] L. Deng, M.G. Payne, and E.W. Hagley, *Opt. Commun.* **198**, 129 (2001).
- [32] A.M. Akulshin, S. Barreiro, and A. Lezama, *Phys. Rev. A* **57**, 2996 (1998).
- [33] S. Chakrabarti, A. Pradhan, B. Ray and Pradip N Ghosh, *J. Phys. B: At. Mol. Opt. Phys.* **38**, 4321 (2005).
- [34] D. Budker and M. Romalis, *Nature Phys.* **3**, 227 (2007).
- [35] S. Bize et al., *J. Phys. B: At. Mol. Opt. Phys.* **38**, S449 (2005).
- [36] Y. Xiao, I. Novikova, D.F. Phillips and R.L. Walsworth, *Phys. Rev. Lett.* **96**, 043601 (2006).
- [37] E. Breschi, G. Kazakov, C. Schori, G. Di Domenico, G. Miletì, A. Litvinov, and B. Matisov, *Phys. Rev. A* **82**, 063810 (2010).
- [38] M. Klein, M. Hohensee, D.F. Phillips and R.L. Walsworth, *Phys. Rev. A* **83**, 013826 (2011).
- [39] P. Meystre and M. Sargent, *Elements of Quantum Optics* (Springer Berlin Heidelberg New York, Berlin Heidelberg, 2007), 4th ed., ISBN 978-3-540-74209-8.
- [40] F.A. Beil, M. Buschbeck, G. Heinze, and T. Halfmann, *Phys. Rev. A* **81**, 053801 (2010).
- [41] R. Liu, W. Yao, and L.J. Sham, *arXiv:1006.5544v1*, (2010).
- [42] A. Batalov, V. Jacques, F. Kaiser, P. Siyushev, P. Neumann, L.J. Rogers, R.L. McMurtrie, N.B. Manson, F. Jelezko, and J. Wrachtrup, *Phys. Rev. Lett.* **102**, 195506 (2009).
- [43] S. Autler and C.H. Townes, *Phys. Rev.* **100**, 703 (1955).
- [44] D.A. Steck, <http://steck.us/alkalidata/> (2009).
- [45] E. Figueroa, F. Vewinger, J. Appel, and A.I. Lvovsky, *Opt. Lett.* **31**, 2625 (2006).
- [46] C. Cohen-Tannoudji and S. Reynaud, *J. Phys. B* **10**, 345 (1977).
- [47] G.S. Agarwal, *Phys. Rev. A* **54**, 3734 (1996).
- [48] D.A. Varshalovich, A.N. Moskalev, and V.K. Khersonskii, *Quantum theory of angular momentum* (World Scientific, 1988).
- [49] V. Boyer, A.M. Marino, R.C. Pooser, and P.D. Lett, *Science* **321**, 544 (2008).
- [50] Q. Glorieux, L. Guidoni, S. Guibal, J.-P. Likforman, and T. Coudreau, *arXiv:1004.3950* (2010).